Propagation length enhancement of surface plasmon polaritons in gold nano-/micro-waveguides by the interference with photonic modes in the surrounding active dielectrics

Research article **Open Access**

Isaac Suárez*, Albert Ferrando, Jose Marques-Hueso, Antonio Díez, Rafael Abargues, Pedro J. Rodríguez-Cantó and Juan P. Martínez-Pastor*

Propagation length enhancement of surface plasmon polaritons in gold nano-/micro-waveguides by the interference with photonic modes in the surrounding active dielectrics

DOI 10.1515/nanoph-2016-0166
Received October 5, 2016; accepted December 21, 2016

Abstract: In this work, the unique optical properties of surface plasmon polaritons (SPPs), i.e. subwavelength confinement or strong electric field concentration, are exploited to demonstrate the propagation of light signal at 600 nm along distances in the range from 17 to 150 μm for Au nanostripes 500 nm down to 100 nm wide (30 nm of height), respectively, both theoretically and experimentally. A low power laser is coupled into an optical fiber tip that is used to locally excite the photoluminescence of colloidal quantum dots (QDs) dispersed in their surroundings. Emitted light from these QDs is generating the SPPs that propagate along the metal waveguides. Then, the above-referred propagation lengths were directly extracted from this novel experimental technique by studying the intensity of light decoupled at the output edge of the waveguide. Furthermore, an enhancement of the propagation length up to 0.4 mm is measured for the 500-nm-wide metal nanostripe, for which this effect is maximum. For this purpose, a simultaneous excitation of the same QDs dispersed in poly(methyl methacrylate) waveguides integrated with the metal nanostructures is performed by end-fire coupling an excitation laser energy as low as 1 KW/cm^2. The proposed mechanism to explain such enhancement is a non-linear interference effect between dielectric and plasmonic (super)modes propagating in the metal-dielectric structure, which can be apparently seen as an effective amplification or compensation effect of the gain material (QDs) over the SPPs, as previously reported in literature. The proposed system and the method to create propagating SPPs in metal waveguides can be of interest for the application field of sensors and optical communications at visible wavelengths, among other applications, using plasmonic interconnects to reduce the dimensions of photonic chips.

Keywords: surface plasmon polariton; propagation length; plasmonic waveguides; loss compensation; polymer waveguides; colloidal quantum dot; gain.

1 Introduction

The ability of metal nanostructures to manipulate light below the diffraction limit can be the basis of the miniaturization and reduction of power consumption of future photonic technology [1]. Such unusual optical property arises from the hybrid electromagnetic wave and charge surface state nature of the surface plasmon polariton (SPP) propagating along metal (or plasmonic) waveguides. SPPs originate from the coupling of incident light to free electrons present in the boundary between a metal and a dielectric, resulting in a subwavelength confined transverse magnetic (TM) wave [2]. This capacity of plasmonic waveguides to concentrate the electromagnetic field at the nanometer scale [3] has been exploited by the scientific community to implement small footprint photonic devices [4] such as surface emitting lasers [5], nanowire edge emitting lasers [6–8], three-dimensional tapers [9],

***Corresponding authors: Isaac Suárez and Juan P. Martínez-Pastor,** UMDO, Instituto de Ciencia de los Materiales, Universidad de Valencia, 46071 Valencia, Spain, e-mail: isaac.suarez@uv.es (I. Suárez); juan.mtnez.pastor@uv.es (J. P. Martínez-Pastor)
Albert Ferrando: Departament d'Òptica i Optometria i Ciències de la Visió, Universitat de València, Dr Moliner, 50, 46100 Burjassot (València), Spain
Jose Marques-Hueso: Institute of Signals, Sensors and Systems (ISSS), Heriot-Watt University, Edinburgh, EH14 4AS, UK
Antonio Díez: Grupo de fibras ópticas y semiconductores, Instituto de Ciencia de los Materiales, Universidad de Valencia, 46071 Valencia, Spain
Rafael Abargues and Pedro J. Rodríguez-Cantó: Intenanomat S.L, C/ Catedrático José Beltrán 2, 46980 Paterna, Spain

multiplexers [10], phase modulators [11], amplitude modulators [12], or photodetectors [13]. The high ohmic losses of the metal, however, restrict the propagation length (Lp) of SPPs to few tens of wavelengths, limiting strongly the practical application of plasmonic waveguides (or plasmonic interconnects) to reduce the final size of future photonic chips.

The demonstration of a lossless propagation SPP by a gain-assisted dielectric material has been studied in plasmonic modes weakly confined in metal films or stripes [14]. Therefore, the loss compensation is based in the high localization of the evanescent field of the mode in the dielectric active medium. For example, the absorption of an SPP travelling along the boundary between a metal and a dielectric has been completely compensated in gold films adjacent to a glass doped with Er ions [15], and partially compensated in silver films by using a polymer doped with dyes [16] or CdSe quantum dots (QD) [17]. Long-range SPPs (LR-SPPs) supported by an insulator-metal-insulator (IMI) structure have attracted more attention for integrated optics because of their higher degree of integration, compatibility with end-fire coupling techniques, and less material gain needed [14]. An important milestone was reached by Gather et al. [18], where LR-SPP travelling along a 4-nm-thin gold film was amplified at 594 nm by using a fluorescent polymer. Thicker metals can improve the confinement of the LR-SPP in the metal in return of higher attenuation. In this way, partial loss compensation (27–32%) was demonstrated in 40–50-nm-thick gold films by using PbS QDs [19, 20], whereas a 50% enhancement was found for the LR-SPP travelling along gold stripes (8-μm wide and 20-nm thick) fabricated on a glass doped with Er ions [21]. On the other hand, complete compensation of losses was reported for a LR-SPP propagating along gold stripes (1-μm wide and 20-nm thick) optically pumped by organic dyes [22, 23]. Finally, silver nanowires of 100 nm in diameter adjacent to organic dyes were proposed to achieve subwavelength confinement but exhibited a weak compensation of losses (14%) [24].

A gain (g) parameter was defined in many of those publications to characterize the enhancement of the LR-SPP intensity. Given that Lp is the inverse of the propagation losses (α) of the LR-SPP ($Lp \approx 1/\alpha$), it is straightforward to define an effective Lp to characterize the LR-SPP enhancement when an active medium surrounding the metal waveguide is optically pumped [23, 24]:

$$Lp_{eff} = \frac{1}{\alpha - g} \quad (1)$$

However, given the high attenuation introduced by metals, the estimation of Lp is usually carried out by indirectly measuring the scattering [17, 18, 24–32] or by decoupling the SPP through additional optical components such as prisms [16], diffraction gratings [15, 22], or more complicated systems as near-field scanning optical microscopes [19, 20, 33].

In this work, we propose a novel method to extract in a direct way the propagation length of LR-SPPs in metal waveguides, both planar and linear at micron and nanoscales. For this purpose, we locally inject light in the SPP by exciting the photoluminescence (PL) of QD dispersed in the surroundings and decouple the signal at their output edge of the metal waveguides. An optical fiber tip is used to provide a small excitation spot selectively placed along the metal structure. This method is validated experimentally and theoretically, because calculated values of Lp in metal nano- and micro-stripes fit very well the measured values. It is worth to highlight the vast range of metal waveguide widths investigated here (100 nm to 10 μm), in order to fill the existing gaps in literature and offer a correct background for our conclusions. In addition, we have demonstrated the enhancement of the propagation length by end-fire coupling a continuous wave (CW) excitation beam into an active dielectric waveguide integrated with the plasmonic nanostructures. As a consequence, excitation fluencies of ≈ 1 KW/cm^2 result in effective propagation lengths as long as 0.4 mm at 600 nm (> 20-fold enhancement) on a 500-nm-wide nanostripe. As a plausible hypothesis, we propose that the measured high gain or effective amplification mechanism is based on a non-linear interference between dielectric and plasmonic modes. Such a mechanism supports our experimental results and could also explain those reported in previous studies in literature, where gain materials were used to compensate the losses in the propagation of LR-SPPs in metal waveguides without amplification of the spontaneous emission [19–22, 24].

2 Experimental

2.1 Structure of the sample

We have designed and fabricated by e-beam [UV] lithography and lift-off 100–1000-nm [5–10 μm]-wide gold metal nanostripes (microstripes) on SiO_2 (2 μm)/Si substrates covered by a poly(methyl methacrylate) (PMMA) film containing core-shell CdSe-ZnS QDs with a filling factor of 1%. Details of QDs and sample fabrication are summarized in Supplementary Information S1, and a scheme of the sample is illustrated in Figure 1A.

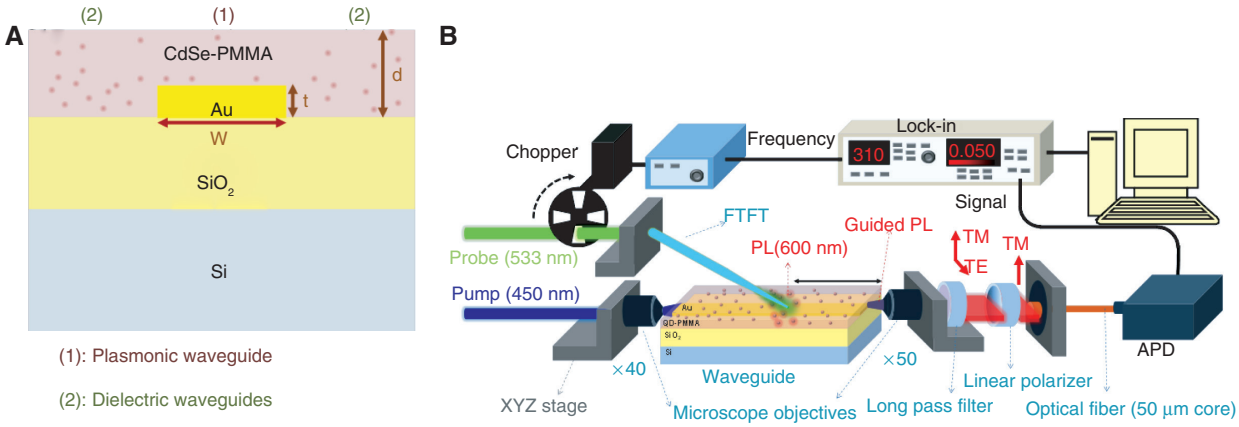

Figure 1: (A) Structure of the sample. (B) Losses of the SPP can be compensated by launching a second pump from the input edge of the sample along the dielectric waveguides located on the left and the right of the stripe. In this experiment, detection and probe beam are synchronized with a lock-in amplifier in order to isolate the light coupled to the SPP from that traveling along the PMMA.

The choice of the gold thickness for the stripe, $t = 30$ nm, obeys a good compromise between propagation losses and mode confinement of the LR-SPP. In addition, the thickness of the nanocomposite film is set to $d = 1$ µm in order to forbid high-order modes in the structure. In these conditions, the Au stripe can propagate the plasmonic LR-SPP in TM polarization, and the cladding dielectric film confines the first TE_0 mode. This photonic mode presents smaller propagation losses due to its weak overlap with the metal. In addition, as the refractive index of PMMA (~1.49) is higher than that of SiO_2 (~1.45), the structures on the left and the right of the stripe (see label 2 in Figure 1A) correspond to dielectric waveguides where light is propagated in both polarizations (TE and TM) with low losses [34]. More details on the design of the metal-dielectric waveguide are given in Supplementary Information S2.

2.2 Experimental set-up

The experimental set-up for the characterization of the propagation length and losses compensation is schematically illustrated in Figure 1B. The excitation probe consisted of a 533-nm wavelength from a CW laser (Z40M18-B, Z-laser Optoelektronic GmbH, Germany) coupled at the input of the fiber tip. Guided PL is collected at the output edge of the waveguide with the aid of a microscope objective and focused at the input of an optical fiber connected to a Photon Counting module supplied by PerkinElmer (France). A long pass filter and a linear polarizer are incorporated after the collection objective in order to eliminate the contribution of the pump beam into the photodetector and select TE and TM polarizations, respectively. Here, the optical fiber core acts as a spatial pin hole to select the LR-SPP signal by minimizing the influence of scattered or radiated light. Metal films or wide stripes (5–10 µm) were characterized with a 20× objective (N.A. = 0.35) and a 200-µm core multi-mode optical fiber. Metal stripes (Thorlabs GmbH, Germany) narrower than 1 µm were studied by using a long working distance with a 50× objective (N.A. = 0.42) and a 50-µm core multi-mode optical fiber in order to provide a higher magnification of the light leaving the exit face of the stripe. Losses compensation experiment is carried out by end-fire coupling a second CW laser coupled at 450 nm at the input edge of the waveguides. In these conditions, the enhancement of the LR-SPP under the extra optical pumping (450 nm) over the probe signal (533 nm) is measured under synchronous detection conditions with a lock-in amplifier (SR810, StandFord Research Systems) (the excitation probe at 532 nm is chopped at 500 Hz for this purpose, as shown in Figure 1B).

3 Characterization of the propagation length in plasmonic waveguides

3.1 Description of the measurement technique

The propagation length (Lp) of the LR-SPP travelling along the waveguide is characterized through the PL generated at the QDs (peak at 600 nm) propagating along the sample, as illustrated in Figure 2A. For this purpose, an excitation beam at 532 nm is coupled through a fused-tapered fiber tip (FTFT) in order to optically pump the

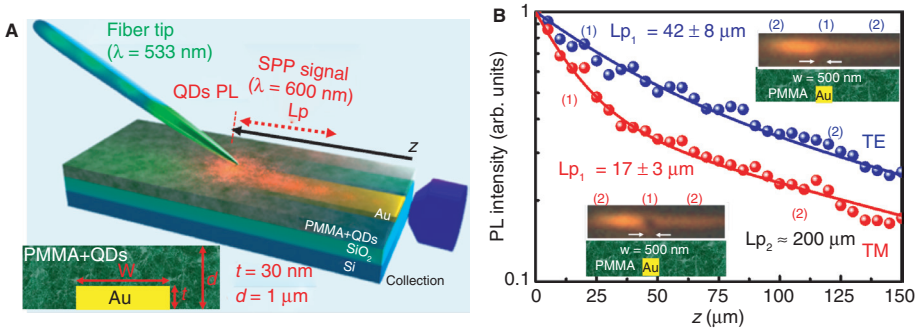

Figure 2: (A) Illustration of the method to directly extract Lp: the fiber tip pumps the QDs (where an external laser at 532 nm is coupled) in a selective region on the top of the Au stripe and the generated PL is coupled to guided modes in the photonic/plasmonic structure. (B) Measured curves of the PL as a function of the distance (z) between the tip and the edge of the sample (symbols) that are fitted (continuous lines) through Equation (2) to extract Lp_1 and Lp_2 for TM (red) and TE (blue) polarizations; images inserted inside the plot window show the cross-section of the light intensity distribution leaving the metal-dielectric waveguide under both polarizations; regions labeled as (1) and (2) identify the space occupied by the metal stripe and the QD-PMM dielectrics, respectively.

nanocrystals above the metal stripe (see Section S3 of Supplementary Information for more details of the FTFT fabrication). As the diameter of the fiber is gradually reduced down to 4 μm [35], the QD-dielectric material is locally excited in a small area (radius of the spot around 2.5 μm) with densities lower than 500 W/cm^2. Then, Lp of the modes supported by the structure is deduced by analyzing the waveguided PL signal at the output edge of the nano-/micro-waveguides as a function of the distance (z) between the tip and the edge of the sample. Figure 2B presents this experimental variation for TE and TM polarizations (data symbols) for an Au nanostripe with width of $w = 500$ nm and height of $t = 30$ nm. These data can be fitted by two exponential decays (continuous lines in Figure 2B):

$$I_{PL} = A_1 \cdot e^{-z/Lp_1} + A_2 \cdot e^{-z/Lp_2}, \quad (2)$$

where A_1 and A_2 are constants. The shortest propagation length for the TM mode was $Lp_1 = 17 \pm 3$ μm, and it should correspond to the "LR-SPP", given that it agrees very well with the theoretical predicted value, 17 μm, as it will be explained in the next section. On the contrary, the shortest decay length for the TE mode (blue curve in Figure 2B) yields $Lp_1 = 42 \pm 8$ μm, which is due to the fact that this mode is centered at the dielectrics (QD-PMMA nanocomposite), hence exhibiting lower losses. The longest propagation length for both polarizations TM and TE, $Lp_2 \approx 200$ μm, corresponds to the dielectric mode and thus exhibits a similar intensity distribution under both polarizations. This picture is consistent with the images included as insets in Figure 2B, which show waveguided PL signal leaving the structure. Region labeled as (1) refers to the light decoupled from the stripe; TM is confined in the metal stripe, while TE corresponds to the dielectric with QDs at the top of the metal stripe. Regions labeled as (2) refer to the dielectric mode with no dependence with polarization. The left side of (2) regions in the inset of Figure 2B appears brighter than the right side, which is mainly attributed to an experimental artifact (e.g. a small shift of the excitation fiber tip or the collection optical fiber).

The proposed method resembles the very well known stripe-excitation experiment, commonly used to characterize gains and losses of active materials in the form of thin films (planar waveguides) [34, 36] but combined with a small area probe that increases the coupling efficiency of photons into SPPs. The FTFT used here as the local excitation source of QDs is similar to others that have been commonly employed to inject/extract light into nanophotonic structures, such as microresonators [35] and nanowires [26–30] by evanescent coupling.

Our method allows the estimation of the propagation length with high accuracy by decoupling waveguided PL light arriving at the output edge of the sample (see the images as insets in Figure 2B). In previous studies, the characterization of the LR-SPP propagation was accomplished through light scattered from the surface of the waveguide [17, 18, 24–32], where Lp was indirectly estimated in silver nanowires [25–27], silver and gold planar films [18, 19], and gold stripes of different lengths [31, 32] by fitting the scattered light measured along the whole waveguides through exponential decays. Other more sophisticated experimental techniques have been proposed in literature, such as decoupling the LR-SPP by either prisms [16] or diffraction gratings [15, 22] or studying the evanescent field along the surface of the waveguide by near-field microscopes [19, 20, 33]. However, the use of prisms is limited to

planar structures, whereas the direct measurement of Lp by diffraction gratings involves the fabrication of several plasmonic waveguides of different lengths to measure the extraction of light on them in order to apply Equation (2) [22]. The characterization by near-field microscopy is strongly limited by the tail of the evanescent field of the plasmonic modes in the air region. Indeed, there are only few works where light was decoupled at the edge of the waveguide but without the estimation of Lp [18, 21].

3.2 Experimental determination of the LR-SPP propagation length in metal waveguides

As the attenuation of the modes depends on the overlap of the plasmonic/photonic signals with the dielectric medium, the geometrical parameters of the plasmonic structure become critical in the propagation properties. In this way, the propagation on metal stripes was studied both experimentally and theoretically in planar structures and metal stripes from $w=10$ μm down to $w=100$ nm. The lateral confinement in a two-dimensional metal structure leads to four fundamental plasmonic modes, as studied by Berini [37, 38]. Among these solutions, there is a two-dimensional counterpart of the LR-SPP mode whose losses decrease with the width of the stripe. Therefore, our experimental characterization demonstrates a reduction of the slope of the curves (and hence the losses) for narrow stripes, as presented in Figure 3A, for widths in the range of $w=250$ nm to $w=5$ μm (results of $w=10$ μm and planar structures are shown in Section S4 of the Supplementary Information). This behavior agrees with previous theoretical studies [38, 39], and it is due to the reduction of the mode confinement in submicron wide metal stripes (see Section S5 of the Supplementary Information). The extracted values of Lp_1 (black circles in Figure 3B) from fitting the experimental data in Figure 3A (and other acquired in more waveguides) to Equation (2) nicely agree with the theoretical calculations (continuous line in Figure 3B) by using the effective refractive index method [40] with refractive indices given by Palik [41] and Johnson and Crysty [42]. The images included as insets in Figure 3B depict the fundamental mode distribution for waveguides of different widths (100–250–500 nm and 1–5 μm) under TM polarization, which perfectly matches the rectangular section occupied by the metal waveguide, as expected from the high attenuation of the LR-SPP propagation as compared to dielectric modes (see also Figure S7b for the mode distribution at $z=0$ and $z=200$ μm in the metal stripe with $w=10$ μm; LR-SPP is significantly attenuated at $z=200$ μm as compared to the dielectric mode intensity). Moreover, the whole area of the LR-SPP mode is spread over the dielectric (see Figure S8), whereas the effective mode area of the light confined in the submicron stripe (dark area in the mode images of Figure 3B) is smaller than λ^2, in agreement with the results obtained by Oulton et al. [43].

It is worth mentioning that the analysis of the propagation length of the LR-SPP at visible wavelengths has been mainly carried out in silver nanostructures [24–30], because of the smaller losses of silver in this wavelength range. The propagation of LR-SPPs along gold waveguides is commonly studied at infrared wavelengths [31, 32], and only a few works are found visible [22]. Although gold presents higher attenuation at short wavelengths, its better stability than silver or aluminum makes it a suitable candidate for all wavelength ranges. Then, the choice of the operation wavelength at 600 nm was not only due to the high quantum yield (gain) of QDs emitting at the visible but also to demonstrate the capability of our method to

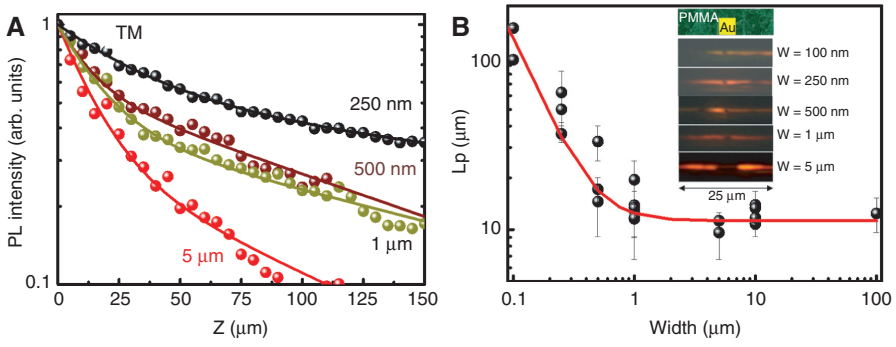

Figure 3: (A) Idem as in Figure 2B but measured in several metal stripes with different widths under TM polarization (data symbols) and the corresponding fits through Equation (2) (continuous lines) to extract propagation length constants. (B) Lp_1 as a function of the waveguide width (data symbols) as compared to values obtained through modeling (continuous line); the inset shows the near-field images measured for different stripes widths under TM polarization.

measure short and long (after compensation) propagation lengths in metal-dielectric waveguiding structures for potential applications in sensing and optical communications at the visible wavelengths. Of course, our experimental technique could be extended to other ranges of wavelengths just by changing the base material (e.g. PbS or PbSe for 1550 nm) of the QDs dispersed inside the polymer [44] and adapting geometrical parameters of the whole photo-plasmonic structure. In particular, our design would present high attenuation in the LR-SPP propagation at infrared wavelengths [45], given that the LR-SPP propagation presents a cut-off for asymmetric structures [38].

3.3 Theory of propagation

The PL generated by the probe excitation of the QD-PMMA nanocomposite is initially coupled to the LR-SPP and the photonic mode supported by the dielectric QD-PMMA waveguide. The coupling efficiency of the spontaneous emission into the different photonic and plasmonic modes depends on the overlap of those modes with the active medium and the excitation profile. A planar metal-dielectric structure can be analyzed by means of the approach based on isotopically oriented dipoles close to a metal slab [46], as previously applied in the study of losses compensation along the propagation of SPPs through films [18] or stripes [23]. As a result, it can be demonstrated that the spontaneous emission of the QDs is mostly transferred to the LR-SPP rather than the short-range SPP or radiated modes (see Section S6 of the Supplementary Information). When two-dimensional stripes are considered, a dielectric mode confined in the PMMA film is also excited. According to the profile of the light at the output of the tip centered at the middle of the stripe and the spatial filtering carried out in our measuring system (collection core fiber of 50 μm and a 50× collection objective), we determine that both modes are excited with similar intensities. Indeed, the best fitting curves in Figures 2B and 3A were obtained with $A_1 \approx A_2$.

Nevertheless, as there is a spatial overlap between the LR-SPP and the waveguide mode, it becomes necessary to introduce coupling through the "dielectric mode to SPP" (q_p) and the "SPP to dielectric mode" (q_p) to solve the system. As a consequence, the metal-dielectric waveguide permits the propagation of one "plasmonic-like" and one "photonic-like" supermode resulting from the linear combination of the LR-SPP and the dielectric modes. Unlike the original LR-SPP and the dielectric modes, the "plasmonic-like" and "photonic-like" supermodes are, by construction, uncoupled. The geometry of the system, however, imposes an asymmetric distribution of the relative intensities of the dielectric and plasmonic components in each supermode, as illustrated in Figure 4. Therefore, "plasmonic-like"

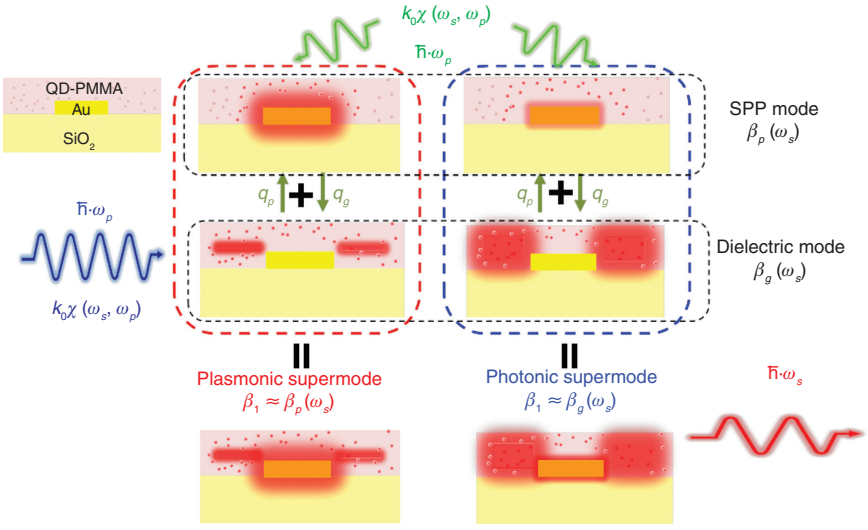

Figure 4: Solution of the propagating (photonic and plasmonic) modes in the waveguide is the result of an energy transfer between the uncoupled SPP and waveguide modes with coupling coefficients, q_p and q_g. Excitation of these modes is carried out by the photoluminescence of QDs embedded in the waveguide. Then, frequency of the probe light at 532 nm is converted to the photoluminescence (600 nm) by the nanostructures [$k_0\chi(\omega_S.\omega_P)$], and light at 600 nm excites the two (plasmonic and photonic) modes allowed in the structure. As the SPP mode presents a higher attenuation, a pump beam at 450 nm coupled at the input edge of the waveguide excites mostly the waveguide mode along the whole length of the waveguide. Again, QDs convert the frequency of the pump beam to that of the PL, and the waveguide mode at 600 nm is fed by a second excitation source. Nevertheless, both photonic and plasmonic modes of the waveguide are influenced by this second source, and as a consequence, their propagation length increases.

and "photonic-like" supermodes resemble the uncoupled LR-SPP and dielectric modes, respectively, and the light intensity leaving the structure can be approximated by Equation (2). Indeed, the respective propagation constants of the LR-SPP [$\beta_p = k_0 \cdot (1.50308 - 0.0025i)$] and plasmonic-like modes [$\beta_1 = k_0 \cdot (1.4971 - 0.0028i)$] are quite similar ($\beta_p \approx \beta_1$). Here k_0 is the wave vector at the wavelength of the PL ($\lambda = 600$ nm).

4 Compensation of losses in the propagation of LR-SPP

4.1 Experimental determination of losses compensation

When the pump beam at 450 nm is end-fire coupled at the input edge of our metal-dielectric waveguides, there is a second source of excitation for the QDs. The high attenuation of the LR-SPP at 450 nm imposes that this second pump beam can only be propagated through the QD-PMMA nanocomposite, where losses are reduced down to 3 cm^{-1} for the filling factor used in this work (1%) [44]. As a consequence, the propagation of the dielectric mode at 450 nm results in the photogeneration of excitons (and hence photons at 600 nm) in the whole length of the QD-PMMA dielectric waveguide (≈ 1 mm), as illustrated in Figure 5A. As a consequence, the decay curve for the waveguided PL intensity under TM (i.e. plasmonic supermode) changes substantially. Indeed, for high enough pump powers (1 KW/cm^2), the losses observed in that mode are reduced down to those in the dielectric medium and curves can be nicely fitted by a single "effective propagation length" as long as 400 ± 200 μm (Figure 5B). This indicates that a certain ratio of the PL signal produced by the optically pumped QDs along the whole metal-dielectric waveguide is transferred to the "plasmonic-like" supermode (and hence to its LR-SPP component) created by the probe, despite the synchronous detection at 600 nm at the modulation frequency of the probe (see set up in Figure 1B).

To the best of our knowledge, such a huge propagation length for a LR-SPP at visible wavelengths is the longest value reported for submicron plasmonic waveguides and the best result obtained under CW optical pumping, where just a partial compensation of losses was only demonstrated in literature [16, 18–21, 24]. It is important to highlight that only a few works are dealing with the compensation of losses along Au linear waveguides at visible wavelengths, where a sufficiently high optical gain was only achieved under pulsed excitation [18, 22].

Therefore, this effective propagation length found in the present work would imply an "effective gain" in the dielectric nanocomposite of around 560 cm^{-1}, according to Equation (1). Nevertheless, the number of electron-hole pairs (excitons) per QD obtained under the optical pumping density used in the experiment (< 10 KW/cm^2) would be $N_{eh} \approx 0.13$; hence, the expected gain in our nanocomposite (with $ff = 10^{-3}$) would be limited to only $g = 0.4$ cm^{-1} (see Section S7 in the Supplementary Information), preventing the compensation of losses by this mechanism. Indeed, stimulated emission of colloidal QDs, as the ones used here, has been only observed under femtosecond pulsed laser pumping in order to avoid the non-radiative Auger recombination [47]. Which is then the mechanism responsible of such an important compensation measured in our experiments?

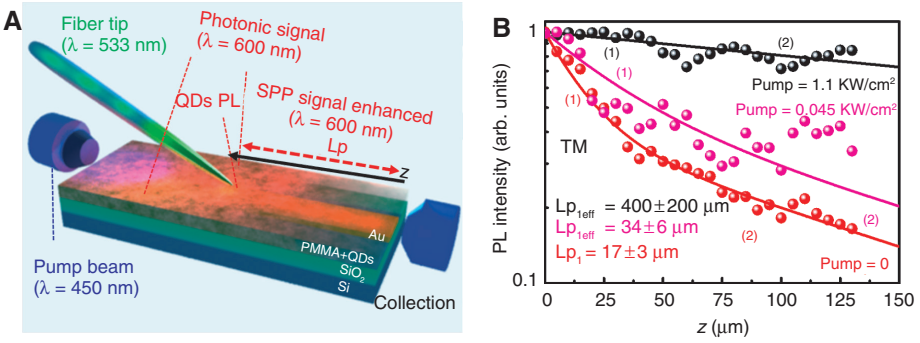

Figure 5: (A) Illustration of the experiment to compensate losses of the SPP propagation by adding a second laser pump (450 nm) from the input edge of the sample; in this case, the probe laser beam (532 nm) coupled to the fiber tip is chopped and light leaving the waveguide is synchronously detected by using a lock-in amplifier in order to isolate the second laser pump. (B) Comparison of data collected without (red solid circles) and with (black solid circles) the extra laser pump to compensate losses and fitting to Equation (2) to extract the effective propagation length.

4.2 Mechanism proposed for the compensation of losses in the LR-SPP propagation

The most plausible explanation for such an unexpected enhancement would be a coherent interference between the LR-SPP and the dielectric modes produced by the superposition of their corresponding "plasmonic-like" and "dielectric-like" supermodes. In these conditions, the intensity measured at the end of the sample propagating in the metal-dielectric waveguide would be approximately given by (details are summarized in Sections S8.1 and S8.2 of the Supplementary Information):

$$I(z) \approx I_P(L) + \left|C_1^T\right|^2 \cdot e^{-\alpha_1 \cdot z} \cdot N_1 + \left|C_2^T\right|^2 \cdot e^{-\alpha_2 \cdot z} \cdot N_2, \quad (3)$$

where $N_1 = \int |e_1|^2 dxdy$ and $N_2 = \int |e_2|^2 dxdy$ are the normalization integrals of supermodes 1 ("plasmonic-like") and 2 ("photonic-like"). $I_p(L)$ is the measured intensity corresponding to the field injected by the pump and propagating along the whole sample length L. It is thus proportional to I_{PUMP}. In a linear approximation, C_1^T and C_2^T are the amplitudes of the electric field injected by the fiber tip into supermodes 1 and 2. The second and third terms in Equation (3) are the contributions to the intensity of these amplitudes after propagating from the tip to the end of the waveguide a distance z. In the synchronized measurement technique used in the experiment, only terms with the temporal modulation on I_{PROBE} are detected, so the first term can be neglected to describe measured values. In this way, Equation (3) reproduces Equation (2) with $A_1 = |C_1^T|^2 \cdot N_1$, $A_2 = |C_2^T|^2 \cdot N_1$, $\alpha_1 = 1/\mathrm{Lp}_1$ and $\alpha_2 = 1/\mathrm{Lp}_2$. Therefore, in accordance with the linear coupled mode theory, A_1 and A_2 are proportional to intensities of the "plasmonic-like" and "photonic-like" supermodes and hence to I_{PROBE}. In addition, and $\mathrm{Lp}_2 = \dfrac{1}{\alpha_2}$ $\mathrm{Lp}_2 = 1/\alpha_2$ are the propagation lengths of these supermodes, which are directly related to the imaginary parts of their complex propagations, so that $\mathrm{Im}(\beta_1) = \dfrac{\alpha_1}{2}$ and $\mathrm{Im}(\beta_2) = \alpha_2/2$, respectively. Remarkably, in a linear approach, they are independent of any pump intensity. Consequently, the observed experimental enhancement of Lp_1 with the pump power cannot be explained by a model based on a linear character of light propagation in the fabricated metal-dielectric waveguides, and hence, some kind of nonlinear mechanism should be introduced.

A suitable candidate for this nonlinear mechanism could be the presence of QDs in the nanocomposite waveguide. Although the exact nature is beyond the scope of this paper, a phenomenological approach is developed here to qualitatively explain the observed enhancement by using a nonlinear generalization of the coupled mode theory (see Section S8.3 in the Supplementary Information). For example, the amplification of stimulated emission under a nonlinear two-photon absorption (TPA) mechanism in waveguides doped with CdSe/CdS/ZnS hetero-QDs has already been demonstrated [48]. Indeed, we observe waveguided photoluminescence under TPA in dielectric waveguides containing our CdSe/ZnS QDs (see Section S8.4 in the Supplementary Information). Furthermore, in similar PMMA-QD waveguides, we demonstrated that it is possible to induce a change in the effective refractive index of the mode at the signal frequency when the active medium is strongly and efficiently pumped at the pump frequency [49], in analogy of a four-wave mixing process [50]. This type of nonlinear modulation can be taken into account by adding an extra term proportional to I_{PUMP} to the waveguide mode propagation constant at the signal frequency, due to the change of its effective refractive index. Consequently, the introduction of a nonlinear mechanism in our originally linear coupled mode theory model would be able to reproduce the dependence of the plasmonic supermode intensity on I_{PUMP} (see Figure S11), which was absent in the linear case.

In mathematical terms, the contribution into supermode 1 of the amplitude injected at the tip shall have now the form $I_1(z, I_{PUMP})$ instead of that predicted by the linear model in Equation (3), in which all coefficients were independent of I_{PUMP}. The behavior of I_1 on I_{PUMP} obtained with the nonlinear model qualitatively agrees with that observed experimentally. It is convenient to define an effective I_{PUMP}-dependent attenuation coefficient for the "plasmonic-like" supermode 1 starting from $I_1(z, I_{PUMP})$ (obtained either from computation or from experimental data). This can be done in the following way:

$$\frac{dI_1(z, I_{PUMP})}{dz} = -\alpha_{1,\mathrm{eff}}(z, I_{PUMP}) \cdot I_1(z, I_{PUMP}), \quad (4)$$

where $\alpha_{1,\mathrm{eff}}(z, I_{PUMP})$ is related with the attenuation (α_1) in the absence of pumping and a newly defined effective gain $g_1(z, I_{PUMP})$ as follows:

$$\alpha_{1,\mathrm{eff}}(z, I_{PUMP}) = \alpha_1 - g_1(z, I_{PUMP}). \quad (5)$$

Then, the effective gain can be calculated as a function of z for each pump power by using Equations (4) and (5), as it is plotted in the right axis of Figure 6A for 1100 (black) and 6 (dark yellow) W/cm^2, respectively. The value results between 300 and 575 cm^{-1}, which is in agreement with the required stimulated emission in the active dielectric nanocomposite to reach such propagation lengths (560 cm^{-1} for the longest Lp) discussed below.

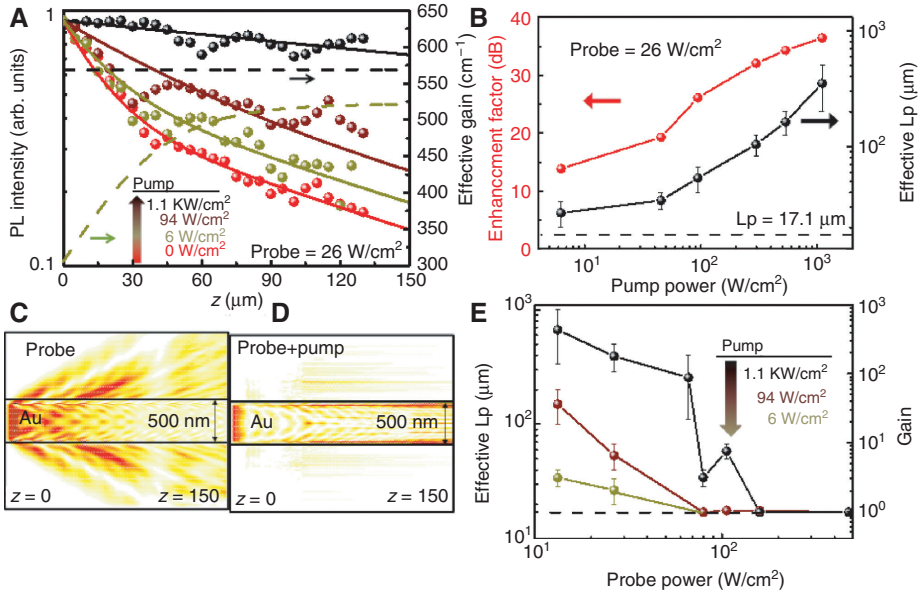

Figure 6: Compensation of LR-SPP losses in a stripe waveguide with $w = 500$ nm. (A) PL intensity as a function of the distance between the tip and the edge of the sample for different pump powers under TM polarization (data symbols); the data are fitted by the model proposed in the text (continuous lines) that is similar to use Equation (2). (B) Enhancement factor in the plasmonic-like supermode as defined in the text (left axis) and effective Lp (right axis) as a function of the pump power, as obtained from (A). BPM simulations of the probe beam propagation without (C) and with the extra colinear laser pumping. (E) Effective Lp_1 (left axis) and corresponding effective gain (right axis) as a function of the power of the probe for different extra laser pump excitation densities.

In general, the behavior of $I_1(z,I_{PUMP})$ differs from a pure exponential. For this reason, the effective attenuation coefficient $\alpha_{1,eff}(z,I_{PUMP})$ is, in general, axially inhomogeneous. For the effective attenuation coefficient, we can define $\overline{\alpha_{1,eff(I_{PUMP})}} = L^{-1}\int_0^L dz_t \alpha_{1,eff}(z,I_{PUMP})$ and the effective propagation length $\overline{Lp_{1,eff}}$, as its inverse. The average effective gain would be simply defined by $\overline{\alpha_{1,eff(I_{PUMP})}} = \alpha_1 - \overline{g_1(I_{PUMP})}$. These average values could be compared to those obtained by fitting the experimental data to a double exponential decay, as was done in Figure 6A (solid lines).

A related quantity to the average effective gain and the other average quantities previously defined is the enhancement factor (left axis in Figure 6B), which, for a given length z, is related with the effective gain and the experimental intensities (see Section S8.5 in the Supplementary Information):

$$EF\,(dB) \approx 10\cdot\log\left(\frac{I_1(z,I_{PUMP})}{I_1(z,0)}\right) = 10\cdot\log\left(e^{-z\cdot(1/\overline{Lp_{1,eff}}-1/Lp_1)}\right) \quad z = 150\ \mu m. \tag{6}$$

Experimentally, the values of $\overline{Lp_{1,eff}}$ for different pump intensities are obtained from the best fits (continuous lines) of experimental data (symbols) in Figure 6A. Note that Lp_1 in Equation (6) is the propagation length in the absence of pumping. The enhancement of the plasmonic-like supermode propagation length, $\overline{Lp_{1,eff}}/Lp_1$, increases up to more than a factor 20 by increasing the production of photons inside the metal-dielectric structure due to the extra optical pumping of QDs (right axis in Figure 6B). A similar conclusion is obtained by means of an active beam propagation method (BPM) [51] to simulate the active plasmonic waveguide embedded in the QD-PMMA nanocomposite. Light travelling along the metal stripe is strongly attenuated (Figure 6C), whereas it is enhanced after the introduction of the pump beam propagation along the dielectric waveguide (Figure 6D). Here the simulations were performed by considering an equivalent effective gain of 560 cm^{-1} in the dielectric medium, as aforementioned.

4.3 Dependence of the intensity of the probe

Results presented in Figures 5B and 6A were obtained with a probe power density of 26 W/cm^2, which is much smaller than the extraoptical pumping used in these experiments. In fact, this should be the condition for a

correct experimental determination of the Lp_1 enhancement for the plasmonic signal. Clearly, one cannot observe compensation of losses for probe intensities higher than 100 W/cm^2, and it becomes necessary to reduce the probe excitation density down to 30 W/cm^2 to observe an intensity enhancement, as shown in Figure 6E. Although lower probe excitation powers seem to give higher Lp_{1eff}, the signal-to-noise ratio decreases significantly, hence a probe power density around 20–30 W/cm^2 was a good compromise to demonstrate an outstanding enhancement of Lp up to more than a factor 20, reaching an effective propagation length for the "plasmonic-like" supermode of around 0.4 mm.

4.4 Dependence of the width of the stripe

As the mode distribution varies with the width of the stripe, the enhancement of Lp_1 will also depend upon this parameter, as observed in Figure 7. The compensation of losses is more important for 500–1000-nm-wide stripes (wine and dark yellow symbols), where an enhancement greater than factor 20 is demonstrated. In addition, it is worth mentioning here that the narrowest stripe studied in this work (w=100 nm) did not present any measurable compensation of losses due to the fact that intrinsic Lp_1 without the extra pumping is very similar to that measured in the active dielectric material (Lp_2). A similar reason can be argued for the weak enhancement observed in the w=250-nm-wide metal stripe (black symbols in Figure 6). In the case of the widest stripe (w=5 μm), the observed enhancement in Lp1 is similar to the previous case, but this time, it is attributed to reduced overlap between the "plasmonic-like" supermode and the active QD-PMMA material.

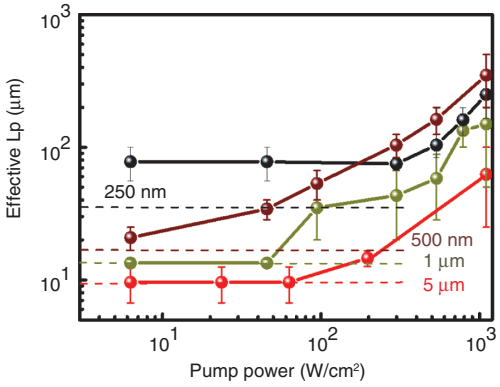

Figure 7: Effective Lp as a function of the pump power for the different widths of the metal stripe.

5 Conclusions

In conclusion, we have proposed the integration of metal nano- and micro-stripes (100 nm–10 μm) with active PMMA waveguides containing CdSe/ZnS core-shell QDs to demonstrate the propagation of LR-SPPs along distances up to 0.4 mm in the case of a 500-nm-wide metal waveguide for which the natural propagation length is 17 μm. Such a long propagation length is achieved by a gain mechanism enhancing the LR-SPP propagation length that is based on a non-linear interference effect between dielectric and plasmonic supermodes propagating along the metal-dielectric structure. For this purpose, an excitation laser beam end-fire coupled at the input edge of the waveguiding structure optically pumps the QDs along its whole length. Light emitted by the QDs under continuous wave (CW) excitation densities in the range 0.01–1 KW/cm^2 feeds the photonic and plasmonic supermodes and generates the nonlinear interference required for enhancing the LR-SPP propagation length. In the present work, we have demonstrated the measurement of propagation lengths associated to photonic and plasmonic modes by means of a novel method based on the local excitation of QDs surrounding the metal stripes, whose PL is generating the LR-SPPs. The present study yielded a good agreement between predicted and measured LR-SPP propagation lengths in different plasmonic waveguides, stripe-like and planar, and hence, it could be applied to other kind of metal-dielectric waveguiding structures. Finally, it is worth mentioning that although the work is focused at 600 nm, it could be extrapolated to other wavelengths just by changing the QD material. The systems studied here, metal-dielectric waveguides, can be elements for future sensing devices, because of the great affinity of gold to many organic molecules, and interconnect for visible optical communication chips, due to the certified enhancement in the propagation length of plasmon polaritons, especially in submicron-size metal stripe waveguides.

Acknowledgments: This work was supported by the Spanish MCINN through projects Nos. TEC2011-29120-C05-01 and TEC2014-53727-C2-1-R, and EU-NAVOLCHI Grant No. 288869. Authors would like to thank Prof. G. Lifante (Universidad Autónoma de Madrid) for his aid in the implementation of the BPM algorithm.

References

[1] Leuthold J, Hoessbacher C, Muehlbrandt S. Plasmonic communications: Light on a wire. Opt Phot News 2013;24:28–35.

[2] Maier SA. Plasmonics: fundamentals and applications, 1st ed. New York, Springer, 2007, xxiv.
[3] Schuller JA, Barnard ES, Cai W, Jun YC, White JS, Brongersma ML. Plasmonics for extreme light concentration and manipulation. Nat Mater 2010;9:193–204.
[4] Gramotnev DK, Bozhevolnyi SI. Plasmonics beyond the diffraction limit. Nat Photonics 2010;4:83–91.
[5] Hill MT, Oei YS, Smalbrugge B, et al. Lasing in metallic-coated nanocavities. Nat Photonics 2007;1:589–94.
[6] Oulton RF, Sorger VJ, Zentgraf T, et al. Plasmon lasers at deep subwavelength scale. Nature 2009;461:629–32.
[7] Lu YJ, Kim J, Chen HJ, et al. Plasmonic nanolaser using epitaxially grown silver film. Science 2012;337:450–53.
[8] Zhang Q, Li G, Liu X, et al. A room temperature low-threshold ultraviolet plasmonic nanolaser. Nat Commun 2014;5:4953.
[9] Choo H, Kim MK, Staffaroni N, et al. Nanofocusing in a metal–insulator–metal gap plasmon waveguide with a three-dimensional linear taper. Nat Photonics 2012;6:838–44.
[10] Ma RM, Yin X, Oulton RF, Sorger VJ, Zhang X. Multiplexed and electrically modulated plasmon laser circuit. Nano Lett 2012;12:5396–402.
[11] Melikyan A, Alloatti L, Muslija A, et al. High-speed plasmonic phase modulators. Nat Photonics 2014;8:229–33.
[12] Haffner C, Heni W, Fedoryshyn Y, et al. All-plasmonic Mach–Zehnder modulator enabling optical high-speed communication at the microscale. Nat Photonics 2015;9:525–8.
[13] Mühlbrandt S, Melikyan A, Harter T, et al. Silicon-plasmonic internal-photoemission detector for 40 Gbit/s data reception. Optica 2016;3:741–7.
[14] Berini P, De Leon I. Surface plasmon–polariton amplifiers and lasers. Nat Photonics 2012;6:16–24.
[15] Krasavin AV, Vo TP, Dickson W, Bolger PM, Zayats AV. All-plasmonic modulation via stimulated emission of copropagating surface plasmon polaritons on a substrate with gain. Nano Lett 2011;11:2231–5.
[16] Noginov MA, Podolskiy VA, Zhu G, et al. Compensation of loss in propagating surface plasmon polariton by gain in adjacent dielectric medium. Opt Express 2008;16:1385–92.
[17] Liu N, Wei H, Li J, et al. Plasmonic amplification with ultra-high optical gain at room temperature. Sci Rep 2013;3:1967.
[18] Gather MC, Meerolz K, Danz N, Leosson K. Net optical gain in a plasmonic waveguide embedded in a fluorescent polymer. Nat Photonics 2010;4:457–61.
[19] Grandidier J, Colas des Francs G, Massenot S, et al. Gain-assisted propagation in a plasmonic waveguide at telecom wavelength. Nano Lett 2009;9:2935–9.
[20] Radko IP, Nielsen MG, Albrektsen O, Bozhevolnyi SI. Stimulated emission of surface plasmon polaritons by lead-sulphide quantum dots at near infra-red wavelengths. Opt Express 2010;18:18633–41.
[21] Ambati M, Nam SH, Ulin-Avila E, Genov DA, Bartal G, Zhang X. Observation of stimulated emission of surface plasmon polaritons. Nano Lett 2008;8:3998–4001.
[22] Kéna-Cohen S, Stavrinou PN, Bradley DDC, Maier SA. Confined surface plasmon–polariton amplifiers. Nano Lett 2013;13:1323–9.
[23] De Leon I, Berini P. Amplification of long-range surface plasmons by a dipolar gain medium. Nat Photonics 2010;4:382–7.
[24] Paul A, Zhen YR, Wang Y, et al. Dye-assisted gain of strongly confined surface plasmon polaritons in silver nanowires. Nano Lett 2014;14:3628–33.
[25] Wild B, Cao L, Sun Y, et al. Propagation lengths and group velocities of plasmons in chemically synthesized gold and silver nanowires. ACS Nano 2012;6:472–82.
[26] Ma Y, Li X, Yu H, Tong L, Gu Y, Gong Q. Direct measurement of propagation losses in silver nanowires. Opt Lett 2010;35:1160–2.
[27] Wang W, Yang Q, Fan F, Xu H, Wang Z. Light propagation in curved silver nanowire plasmonic waveguides. Nano Lett 2011;11:1603–8.
[28] Dong CH, Ren XF, Yang R, et al. Coupling of light from an optical fiber taper into silver nanowires. Appl Phys Lett 2009;95:221109.
[29] Tian J, Ma Z, Li Q, et al. Nanowaveguides and couplers based on hybrid plasmonic modes. Appl Phys Lett 2010;97:231121.
[30] Guo X, Qiu M, Bao J, et al. Direct coupling of plasmonic and photonic nanowires for hybrid nanophotonic components and circuits. Nano Lett 2009;9:4515–9.
[31] Flynn RA, Bussmann K, Simpkins BS, Vurgaftman I, Kim CS, Long JP. Propagation length of surface plasmon polaritons determined by emission from introduced surface discontinuities. J Appl Phys 2010;107:013109.
[32] Bracher G, Schraml K, Jakubeit C, Kaniber M, Finley JJ. Direct measurement of plasmon propagation lengths on lithographically defined metallic waveguides on GaAs. J Appl Phys 2011;110:123106.
[33] Zia R, Schulle JA, Brongersma ML. Near-field characterization of guided polariton propagation and cutoff in surface plasmon waveguides. Phys Rev B 2006;74:165415.
[34] Gordillo H, Suárez I, Abargues R, Rodríguez-Cantó PJ, Martínez-Pastor JP. Color tuning and white light by dispersing cdse, cdte, and cds in pmma nanocomposite waveguides. IEEE Photon J 2013;5:2201412.
[35] Arques L, Carrascosa A, Zamora V, Díez A, Cruz JL, Andrés MV. Excitation and interrogation of whispering-gallery modes in optical microresonators using a single fused-tapered fiber tip. Opt Lett 2011;36:3452–4.
[36] Dal Negro L, Bettotti P, Cazzanelli M, Pacifi D, Pavesi L. Applicability conditions and experimental analysis of the variable stripe length method for gain measurements. Opt Commun 2004;229:337–48.
[37] Berini P. Long-range surface plasmon polaritons. Adv Opt Photonics 2009;1:484–588.
[38] Berini P. Plasmon-polariton waves guided by thin lossy metal films of finite width: Bound modes of asymmetric structures. Phys Rev B 2001;63:125417.
[39] Zia R, Selker MD, Brongersma ML. Leaky and bound modes of surface plasmon waveguides. Phys Rev B 2005;71:165431.
[40] Lifante G. Integrated photonics. Fundamentals, 1st ed. USA: John Wiley & Sons. 2003.
[41] Palik ED. Handbook of optical constants of solids. The Netherlands: Elsevier. 1997.
[42] Johnson PB, Christy RW. Optical constants of the noble metals. Phys Rev B 1972;6:4370.
[43] Oulton RF, Sorger VJ, Genov DA, Pile DFP, Zhang XA. A hybrid plasmonic waveguide for subwavelength confinement and long-range propagation. Nat Photonics 2008;2:496–500.

[44] Suárez I, Gordillo H, Abargues R, Albert S, Martínez-Pastor JP. Photoluminescence waveguiding in CdSe and CdTe QDs–PMMA nanocomposite films. Nanotechnology 2011;22:435202.
[45] Boltasseva A, Nikolajsen T, Leosson K, Kjaer K, Larsen MS, Bozhevolnyi SI. Integrated optical components utilizing long-range surface plasmon polaritons. J Lightwave Technol 2005;23:413–22.
[46] Barnes WL. Fluorescence near interfaces: The role of photonic mode density. J Mod Opt 2009;45:661–99.
[47] Klimov VI, Mikhailovsky AA, Xu S, et al. Optical gain and stimulated emission in nanocrystal quantum dots. Science 2000;290:314–7.
[48] Jasieniak JJ, Fortunati I, Gardin S, et al. Highly efficient amplified stimulated emission from CdSe-CdS-ZnS quantum dot doped waveguides with two-photon infrared optical pumping. Adv Mater 2008;20:69–73.
[49] Hervás J, Suárez I, Pérez J, et al. MWP phase shifters integrated in PbS-SU8 waveguides. Opt Express 2015;23:14351–9.
[50] Mecozzi A, Mork J, Hofmann M. Transient four-wave mixing with a collinear pump and probe. Opt Lett 2005;21:1017–9.
[51] Gordillo H, Suárez I, Abargues R, Rodríguez-Cantó PJ, Almuneau G, Martínez-Pastor JP. Quantum-dot double layer polymer waveguides by evanescent light coupling. J Lightwave Technol. 2013;31:2515–25.

Supplemental Material: The online version of this article (DOI: 10.1515/nanoph-2016-0166) offers supplementary material, available to authorized users.